JOURNAL OF COMPUTATIONAL PHYSICS **136,** 503–521 (1997)
ARTICLE NO. CP975778

Modelling of Two-Phase Flow with Second-Order Accurate Scheme

Iztok Tiselj and Stojan Petelin

Jožef Stefan Institute, Jamova 39, Ljubljana, 1111, Slovenia
E-mail: iztok.tiselj@ijs.si

Received June 3, 1996; revised May 28, 1997

A second-order accurate scheme based on high-resolution shock-capturing methods was used with a typical two-phase flow model which is used in the computer codes for simulation of nuclear power plant accidents. The two-fluid model, which has been taken from the computer code RELAP5, consists of six first-order partial differential equations that represent 1D mass, momentum, and energy balances for vapour and liquid. The partial differential equations are ill-posed—nonhyperbolic. The hyperbolicity required by the presented numerical scheme was obtained in the practical range of the physical parameters by minor modification of the virtual mass term. No conservative form of the applied equations exists, therefore, instead of the Riemann solver, more basic averaging was used for the evaluation of the Jacobian matrix. The equations were solved using nonconservative and conservative basic variables. Since the source terms are stiff, they were integrated with time steps which were shorter than or equal to the convection time step. The sources were treated with Strang splitting to retain the second-order accuracy of the scheme. The numerical scheme has been used for the simulations of the two-phase shock tube problem and the Edwards pipe experiment. Results show the importance of the closure laws which have a crucial impact on the accuracy of two-fluid models. Advantages of the second-order accurate schemes are evident especially in the area of fast transients dominated by acoustic phenomena.

1. INTRODUCTION

Safety analyses of nuclear reactors require computations of complex two-phase flows. RELAP5 computer code [6, 2, 35] is one of the few codes (CATHARE [3], TRAC [33]) that were created for this purpose. The current version of the code describes two-phase flow with a six-equation two-fluid model. The equations are one-dimensional since the direction of the flow is clearly defined. The system of the six first-order partial differential equations is derived from the cross-section averaged Navier–Stokes equations [4, 12, 2]. Diffusion terms with second-order derivatives are replaced by empirical correlations which are flow regime dependent. The type of the flow regime is determined by the flow parameters and the geometry. The basic RELAP5 equations are ill-posed, nonhyperbolic with complex eigenvalues, while the discretized equations are well-posed [25]. The ill-posedness of the discretized equations in RELAP5 is avoided by the first-order accurate numerical scheme which is based upon a semi-implicit finite difference method with staggered grid and donor-cell discretization of the convective terms [35]. The main advantages of such a scheme are robustness and efficiency. The weak side of the scheme is its numerical dissipation, which tends to smear discontinuities on coarse grids. Numerical dissipation cannot be easily avoided with the existing type of the scheme, since this dissipation presents the main mechanism which removes the ill-posedness from the discretized equations and ensures the scheme's stability. The RELAP5 code successfully covers the area of the transients with characteristic time scale determined by the fluid velocity [27], but it has to be used with extreme caution for transients with acoustic waves [21].

The main directions of the development of today's two-phase flow models are: improvement of the mathematical models (better closure models, from 1D into 3D) and improvement of the numerical methods. To obtain optimum results, parallel improvement in both fields is necessary. This paper presents the application of an advanced numerical scheme using the existing two-fluid model of RELAP5 computer code; however, we believe that this type of numerical schemes will also be useful for the next generation of mathematical models of two-phase flow.

The most important contributions in the field of second-order accurate methods for two-phase flows were previously concentrated on the construction of Roe's approximate Riemann solver [23]. Toumi [30] presented a weak formulation of Roe's approximate Riemann solver for the homogeneous equilibrium two-phase flow, and later [31, 32] applied this solver to a simple two-fluid model of two-phase flow. However, he concluded that solution of the Riemann problem is unknown for the nonconservative systems and that there is no exact solver available to check the validity of the presented numerical solutions and the speed of the computed discontinuities.

This article attempts to emphasize the most important aspects of the two-phase flow modelling with second-order accurate schemes and to offer some possible answers to the questions: When is it meaningful to apply a second-order accurate scheme for the presented two-fluid model with limited reliability of the applied empirical correla-

0021-9991/97 $25.00

tions? How to write the basic equations? How to evaluate characteristic velocities? How to treat source terms? The basic equations and closure models are described in Section 2. In Sections 3 and 4 it is shown how to ensure the hyperbolicity of the two-fluid models, which is required for the application of the presented second-order numerical scheme. The numerical method is presented in Section 5, and treatment of the sources in Section 6. The model of the single to two-phase flow transition is discussed in Section 7. In Section 8 behaviour of the discontinuous solutions is analyzed. Sections 9 and 10 present two-phase shock tube results and results of the Edwards experiment.

2. BASIC EQUATIONS

The basic mathematical model considered in this paper is a six-equation equal-pressure two-fluid model used in computer code RELAP5. The basic equations are mass, momentum, and energy balances for the dispersed flow of vapour and liquid [6] with equal phasic pressures. The 1D equations are written in a form which allows for a smooth change of the pipe cross-section:

$$\frac{\partial(1-\alpha)\rho_f}{\partial t}+\frac{1}{A}\frac{\partial(1-\alpha)\rho_f v_f A}{\partial x}=-\Gamma_g, \tag{1}$$

$$\frac{\partial\alpha\rho_g}{\partial t}+\frac{1}{A}\frac{\partial\alpha\rho_g v_g A}{\partial x}=\Gamma_g, \tag{2}$$

$$\begin{aligned}(1-\alpha)\,\rho_f\frac{\partial v_f}{\partial t}+\frac{1}{2}(1-\alpha)\rho_f\frac{\partial v_f^2}{\partial x}&\\ =-(1-\alpha)\frac{\partial p}{\partial x}+(1-\alpha)\rho_f g\cos\theta&\\ -\frac{1}{2}(1-\alpha)\rho_f\frac{f_{wf}}{D}|v_f|v_f&\\ -\Gamma_g(v_i-v_f)+\frac{C_D}{8}\rho_c a_{gf}|v_r|v_r+CVM,&\end{aligned} \tag{3}$$

$$\begin{aligned}\alpha\rho_g\frac{\partial v_g}{\partial t}+\frac{1}{2}\alpha\rho_g\frac{\partial v_g^2}{\partial x}&=-\alpha\frac{\partial p}{\partial x}+\alpha\rho_g g\cos\theta\\ &-\frac{1}{2}\alpha\rho_g\frac{f_{wg}}{D}|v_g|v_g+\Gamma_g(v_i-v_g)\\ &-\frac{C_D}{8}\rho_c a_{gf}|v_r|v_r-CVM,\end{aligned} \tag{4}$$

$$\begin{aligned}\frac{\partial(1-\alpha)\rho_f u_f}{\partial t}+\frac{1}{A}\frac{\partial(1-\alpha)\rho_f u_f v_f A}{\partial x}&\\ =-p\frac{\partial(1-\alpha)}{\partial t}-\frac{p}{A}\frac{\partial(1-\alpha)v_f A}{\partial x}+Q_{if}&\\ -\Gamma_g h_f^*+\frac{1}{2}(1-\alpha)\rho_f\frac{f_{wf}}{D}v_f^2|v_f|,&\end{aligned} \tag{5}$$

$$\begin{aligned}\frac{\partial\alpha\rho_g u_g}{\partial t}+\frac{1}{A}\frac{\partial\alpha\rho_g u_g v_g A}{\partial x}&\\ =-p\frac{\partial\alpha}{\partial t}-\frac{p}{A}\frac{\partial\alpha v_g A}{\partial x}+Q_{ig}+\Gamma_g h_g^*&\\ +\frac{1}{2}\alpha\rho_g\frac{f_{wg}}{D}v_g^2|v_g|.&\end{aligned} \tag{6}$$

Index f refers to the liquid phase and index g to the gas phase. Nomenclature has not been typed, however, most of the variables are described in text and Table 1. Two additional equations of state for each phase are needed to close the system of equations. The equation of state for phase k is

$$\begin{aligned}d\rho_k&=\left(\frac{\partial\rho_k}{\partial p}\right)_{u_k}dp+\left(\frac{\partial\rho_k}{\partial u_k}\right)_p du_k,\\ \left(\frac{\partial\rho_k}{\partial p}\right)_{u_k}&=\frac{c_{pk}\kappa_k\rho_k-T_k\beta_k^2}{c_{pk}-p\beta_k/\rho_k},\\ \left(\frac{\partial\rho_k}{\partial p}\right)_p&=-\frac{\beta_k\rho_k}{c_{pk}-p\beta_k/\rho_k}.\end{aligned} \tag{7}$$

Partial derivatives in Eq. (7) are expressed by variables which are determined by the RELAP5 subroutines of water properties using pressure and specific internal energy as an input.

The terms in Eqs. (1)–(6), which require additional closure models, can be separated into two groups:

(I) *Differential terms* contain derivatives and influence the character of the equations. The only differential model applied in Eqs. (1)–(6) is the virtual mass term *CVM* in momentum equations (3) and (4). It contains derivatives of the phasic velocities v_f, v_g and is described in Section 3.

(II) *Nondifferential terms* (see Table I). Their closure models do not contain derivatives. Nondifferential terms can be further divided into two groups on the basis of their characteristic time scales:

(i) Terms for interphase exchanges with characteristic time scales shorter than the acoustic time scale (terms with Γ_g, Q_{if}, Q_{ig}, C_D). These terms require special treatment in the numerical schemes.

(ii) Terms for fluid–wall interactions (wall friction, wall–fluid heat exchange) and volumetric forces with long characteristic time scales which do not present any difficulty for the numerical schemes. For this reason we neglected wall-to-fluid heat exchange terms in the energy equations (5) and (6) in our code named PDE2 (partial differential equations 2nd order). Tests have shown that wall friction terms can also be neglected in the transients presented in this paper. The correlations used in the tests

TABLE I

Nondifferential Closure Models in Two-Fluid Model, Eqs. (1)–(6)

$C_D = 24(1 + 0.1Re_k^{0.75})/Re_k$ interphase drag coefficient [6, 13],
$Re_k = v_r d_0 \rho_c/\mu_c$ Reynolds number of bubbles or droplets,
d_0 average bubble/droplet diameter, $d_0 = d_{\max}/2$, $d_{\max} = We_{\text{critical}}\sigma/\rho_c v_r^2$

$a_{gf} = 3.6\,\alpha_d/d_0$ interfacial area per unit volume [6, 37],
$\alpha_d = \alpha$ in bubbly flow and $\alpha_d = (1 - \alpha)$ in droplet flow

$\Gamma_g = -(Q_{if} + Q_{ig})/(h_g^* - h_f^*)$ vapour source
$Q_{if} = H_{if}(T_s - T_f)$, $Q_{ig} = H_{ig}(T_s - T_g)$ interface heat transfer terms
H_{if}, H_{ig} liquid-interface and gas-interface heat transfer coeff. per unit volume
Bubbly flow:
$(H_{if})_{superheated}$ = max(Plesset-Zwick correlation [6, 22], modified Lee-Ryley [6, 15])
$(H_{if})_{subcooled}$ = Unal correlation [6, 36]
$(H_{ig})_{superheated,subcooled} = Na_{gf}$, N constant [6, 5]
Droplet flow:
$(H_{if})_{superheated,subcooled} = Nk_f a_{gf}/d_0$ [6]
$(H_{ig})_{superheated}$ = Lee-Ryley correlation [6, 15]
$(H_{ig})_{subcooled} = Ma_{gf}$, M constant [6]

$v_i = v_g$ during condensation and $v_i = v_f$ during vaporization or in equilibrium.

f_w = Colebrook correlation [7]—friction factors
bubbly flow: f_{wf} = Colebrook correlation, $f_{wg} = 0$
droplet flow: f_{wg} = Colebrook correlation, $f_{wf} = 0$

for the f_{wf} and f_{wg} coefficients in wall friction terms of momentum equations (3) and (4) present a simplification of the RELAP5 correlations described in [6].

Most of the closure laws in RELAP5 are flow regime dependent. Two basic groups of flow regimes in RELAP5 are flow regimes in horizontal and vertical pipes. RELAP5 recognizes five flow regimes in horizontal pipes: bubbly, slug, annular-mist, droplet, and horizontally stratified flow regime. The type of the flow regime in horizontal flows is determined by the relative interphase velocity v_r and vapour volume fraction α. Similar flow regimes can be met in vertical pipes (the closure laws are not necessarily the same), where mixture velocity and the vapour volume fraction determine the flow regime [19]. An additional set of so-called postdryout flow regimes is present in vertical pipes when pipe surface temperatures and heat fluxes are too high to allow surface wetting [6]. Exact modelling of all the flow regimes described in RELAP5 would be a very hard and time-consuming task and would be justified only in the case when a new code version might be produced. In the PDE2 code with second-order accurate scheme, as presented in this paper, two flow regimes were modelled (see Table I): bubbly ($\alpha \leq 0.5$) and droplet ($\alpha \geq 0.95$) regimes of two-phase flow. Interpolation of the parameters has been used for the intermediate vapour volume fractions ($0.5 < \alpha < 0.95$). These correlations were used because they present the simplest complete flow regime map in RELAP5 which is valid for highly dispersed flows. However, we used the same correlations also for the situations in which some other flow regimes might appear. The complete set of applied correlations is still very comprehensive and is therefore not presented here. Survey of the applied correlations for C_D, a_{gf}, H_{if}, H_{ig} is collected in Table I, while the details can be found in [6]. Although we used the simplest flow regime map, the correlations represented one-third of our code.

3. HYPERBOLICITY OF THE EQUATIONS

The basic equations of the equal-pressure two-fluid models often present an ill-posed problem with complex eigenvalues of the Jacobian matrix [6, 25]. However, additional differential terms—which are usually added into the basic equations—can make the equations well-posed.

An additional differential term which is usually taken into account in the momentum equations of the 1D two-fluid models is the virtual mass term. The virtual mass term represents the interphase force which appears as a consequence of the different phasic accelerations and can be analytically derived for a single solid sphere (bubble or drop) in inviscid flow [37]. The form of the virtual mass term in realistic two-phase flows is not known exactly, and thus, different computer codes for nuclear thermal hydraulics simulations [6, 3, 33] use different forms of the virtual mass term. The most general form of the virtual

mass given by Drew *et al.* [8] contains the following derivatives:

$$CVM \propto C_{vm}\left(\frac{\partial v_g}{\partial t} + v_f\frac{\partial v_g}{\partial x} - \frac{\partial v_f}{\partial t} - v_g\frac{\partial v_f}{\partial x} + (1-\lambda)(v_g - v_f)\frac{\partial (v_f - v_g)}{\partial x}\right), \tag{8}$$

where the parameter λ should be a function of the vapour volume fraction with value 2 for $\alpha \to 0$ and 0 for $\alpha \to 1$. In the RELAP5 code, the parameter λ is set equal to 1; however, due to problems with the RELAP5 numerical scheme, all spatial derivatives were also neglected:

$$CVM_{\text{RELAP5}} = C_{vm}\alpha(1-\alpha)\rho_m\frac{\partial v_r}{\partial t}. \tag{9}$$

The basic equations with that type of the virtual mass term are still ill-posed, and so we retained the spatial derivatives in the virtual mass term:

$$CVM_{\text{PDE2}} = C_{vm}\alpha(1-\alpha)\rho_m\left(\frac{\partial v_g}{\partial t} + v_f\frac{\partial v_g}{\partial x} - \frac{\partial v_f}{\partial t} - v_g\frac{\partial v_f}{\partial x}\right). \tag{10}$$

The hyperbolicity of the equations with *CVM* (10) was achieved in our PDE2 code by minor modification of the RELAP5 virtual mass coefficient C_{vm} [38]:

$$C_{vm\text{-RELAP5}} = \begin{cases} \dfrac{1+2\alpha}{2-2\alpha}, & \alpha < 0.5, \\ \dfrac{3-2\alpha}{2\alpha}, & \alpha > 0.5, \end{cases} \quad \to$$

$$C_{vm\text{-PDE2}} = \begin{cases} (1+2\alpha)/(2-2\alpha), & \alpha < 0.5, \\ \sqrt{\left(\dfrac{3-2\alpha}{2\alpha}\right)^2 - \dfrac{(\alpha-1)(2\alpha-1)}{(1+\alpha\rho_g/\rho_f-\alpha)^2}}, & \alpha > 0.5. \end{cases} \tag{11}$$

This correction of the virtual mass coefficient is based on the approximate analytical expressions for the Jacobian eigenvalues (Section 4, Eq. (15)) derived with the assumption of mixture incompressibility [28]. The form of the virtual mass coefficient derived on the basis of such assumption does not guarantee unconditional hyperbolicity of the equations, i.e., complex eigenvalues can appear at extremely large relative interphase velocities v_r which are comparable to the sonic velocity: $v_r \gtrsim 0.3c$.

Another additional differential term is often used in momentum equations of the computer codes for thermal hydraulics—the interface pressure term $P_i\nabla\alpha$. It is clearly derived in stratified flows, $P_i = \alpha(1-\alpha)(\rho_f - \rho_g)gD$, and is used in stratified flow regimes in RELAP, CATHARE, and TRAC codes [6, 3, 33]. Parameter P_i is called the interface pressure, even though it is not the actual pressure on the interface and should not be confused with the pressure on the interfacial surface when the interface pressure term is written in the form $(p_{ki} - p_k)\nabla\alpha$ [24]. The role of the interface pressure term in nonstratified flows is rather controversial, as can be seen from a paper by Sha and Soo [24] who collected different views on the role of the interface pressure term. There is no interface pressure term in nonstratified flow regimes of RELAP5 code, while CATHARE code [3] uses the $P_i\nabla\alpha$ term in nonstratified flows to ensure the hyperbolicity of the equations. Toumi [31] attempted to apply an approximate Riemann solver for Eqs. (1)–(6), where the *CVM* term in Eqs. (3) and (4) has been replaced with the interface pressure taken from CATHARE:

$$P_i\frac{\partial\alpha}{\partial x}, \quad P_i = \frac{\delta_i\alpha(1-\alpha)\rho_g\rho_f v_r^2}{\alpha\rho_f + (1-\alpha)\rho_g}. \tag{12}$$

This correlation does not have any physical background, but it does ensure the hyperbolicity of the equations for $\delta_i \geq 1$ and $v_r \lesssim 0.3c$.

The transients presented in this paper are analyzed by the RELAP5 two-fluid model with virtual mass term (10). Since any differential closure model can be applied in two-fluid models, some results are presented also for the two-fluid model with interface pressure term (12) in order to check the role of the additional differential terms.

4. APPROXIMATE EIGENVALUES AND EIGENVECTORS

The system of Eqs. (1)–(6) represents the conservation laws; however, it cannot be written in the conservative form due to the pressure gradient terms and additional differential terms. The equations are therefore written in the nonconservative form,

$$\mathbf{A}\frac{\partial\boldsymbol{\Psi}}{\partial t} + \mathbf{B}\frac{\partial\boldsymbol{\Psi}}{\partial x} = \mathbf{S}, \tag{13}$$

where $\boldsymbol{\Psi}$ represents the vector of the nonconservative variables $\boldsymbol{\Psi} = (p, \alpha, v_f, v_g, u_f, u_g)$. For evaluation of the approximate eigenvalues the enthalpy form of the energy equations with $\boldsymbol{\Psi} = (p, \alpha, v_f, v_g, h_f, h_g)$ is more convenient. In this case the system eigenvalues are given by the determinant $\det(B - \lambda A) = 0$:

$$\mathrm{Det}\begin{vmatrix} (1-\alpha)\frac{\partial \rho_f}{\partial p}(v_f-\lambda) & -\rho_f(v_f-\lambda) & (1-\alpha)\rho_f & 0 & (1-\alpha)\frac{\partial \rho_f}{\partial h_f}(v_f-\lambda) & 0 \\ \alpha\frac{\partial \rho_g}{\partial p}(v_g-\lambda) & \rho_g(v_g-\lambda) & 0 & \alpha\rho_g & 0 & \alpha\frac{\partial \rho_{fg}}{\partial h_g}(v_g-\lambda) \\ 1-\alpha & P_i & (1-\alpha)\rho_f(v_f-\lambda)+W(v_g-\lambda) & -W(v_f-\lambda) & 0 & 0 \\ \alpha & -P_i & -W(v_g-\lambda) & \alpha\rho_g(v_g-\lambda)+W(v_f-\lambda) & 0 & 0 \\ -\frac{v_f-\lambda}{\rho_f} & 0 & 0 & 0 & v_f-\lambda & 0 \\ -\frac{v_g-\lambda}{\rho_g} & 0 & 0 & 0 & 0 & v_g-\lambda \end{vmatrix} = 0. \tag{14}$$

with $W = C_{vm}\alpha(1-\alpha)\rho_m$.

RELAP5 eigenvalues are obtained if P_i is set equal to zero, and eigenvalues of the Toumi model with an interface pressure term are obtained if W is set equal to zero. Two trivial eigenvalues are $\lambda_5 = v_f$ and $\lambda_6 = v_g$. Fields belonging to $\lambda_{5,6}$ are linearly degenerate. If incompressibility of both phases is assumed, all partial derivatives of densities are equal to zero, and two approximate eigenvalues for the RELAP5 equations derived by Trapp and Ransom [34] are obtained:

$$\lambda_{3,4} = \frac{[(1-\alpha)\rho_g + C_{vm}\rho_m/2]v_g + [\alpha\rho_f + C_{vm}\rho_m/2]v_f \pm \sqrt{\Delta}v_r}{\alpha\rho_f + (1-\alpha)\rho_g + C_{vm}\rho_m},$$
$$\Delta = (C_{vm}\rho_m/2)^2 - \alpha(1-\alpha)\rho_f\rho_g. \tag{15}$$

These two eigenvalues are real for positive Δ and are always between λ_5 and λ_6; i.e., if $\lambda_{5,6} > 0$ then $\lambda_{3,4} > 0$. A similar procedure for the equations with interface pressure term yields

$$\lambda_{3,4} = \frac{(1-\alpha)\rho_g v_g + \alpha\rho_f v_f \pm \sqrt{\Delta}v_r}{\alpha\rho_f + (1-\alpha)\rho_g},$$
$$\Delta = (\delta_i - 1)\alpha(1-\alpha)\rho_f\rho_g. \tag{16}$$

In this case third and fourth eigenvalues do not necessarily lie between the phasic velocities, and it may even happen that for $\lambda_{5,6} > 0$ one of the eigenvalues λ_3 or λ_4 becomes negative. Characteristic fields of $\lambda_{3,4}$ are genuinely nonlinear.

The first and second eigenvalues, which correspond to the fastest sonic characteristics are obtained from the exact characteristic polynomial (14) and known roots λ_3 to λ_6. The expressions for λ_1 and λ_2 are long and are not presented here. Only two-phase sonic velocity is given instead. The expression for the sonic velocity can be obtained if both phasic velocities are set equal to zero in the determinant (14):

$$c^2 = \frac{\rho_f\rho_g}{\dfrac{\alpha\rho_f}{c_g^2} + \dfrac{(1-\alpha)\rho_g}{c_f^2}} \frac{C_{vm}\rho_m + \alpha\rho_f + (1-\alpha)\rho_g}{C_{vm}\rho_m^2 + \rho_f\rho_g},$$
$$c_f^{-2} = \left(\frac{\partial \rho_f}{\partial p}\right)_{h_f} + \frac{1}{\rho_f}\left(\frac{\partial \rho_f}{\partial h_f}\right)_p, \quad c_g^{-2} = \left(\frac{\partial \rho_g}{\partial p}\right)_{h_g} + \frac{1}{\rho_g}\left(\frac{\partial \rho_g}{\partial h_g}\right)_p. \tag{17}$$

One can see that the virtual mass term does appear in (17), while the interface pressure term—which contains only the spatial derivatives of the vapour volume fraction—does not affect the sonic velocity.

Another interesting insight into the two-phase flow equations is given by the approximate eigenvectors. The structure of the eigenvectors matrix can be written as

$$\mathbf{L} = |\mathbf{l}_1\,\mathbf{l}_2\,\mathbf{l}_3\,\mathbf{l}_4\,\mathbf{l}_5\,\mathbf{l}_6| = \begin{vmatrix} / & / & q_{13}v_r^2 & q_{14}v_r^2 & 0 & 0 \\ / & / & 1 & 1 & 0 & 0 \\ / & / & q_{33}v_r & q_{34}v_r & 0 & 0 \\ / & / & q_{43}v_r & q_{44}v_r & 0 & 0 \\ / & / & q_{13}v_r^2/\rho_f & q_{14}v_r^2/\rho_f & 1 & 0 \\ / & / & q_{13}v_r^2/\rho_g & q_{14}v_r^2/\rho_g & 0 & 1 \end{vmatrix}. \tag{18}$$

The exact form of the first and second eigenvectors which correspond to the sonic eigenvalues is not given since it does not concern the general properties of the equations.

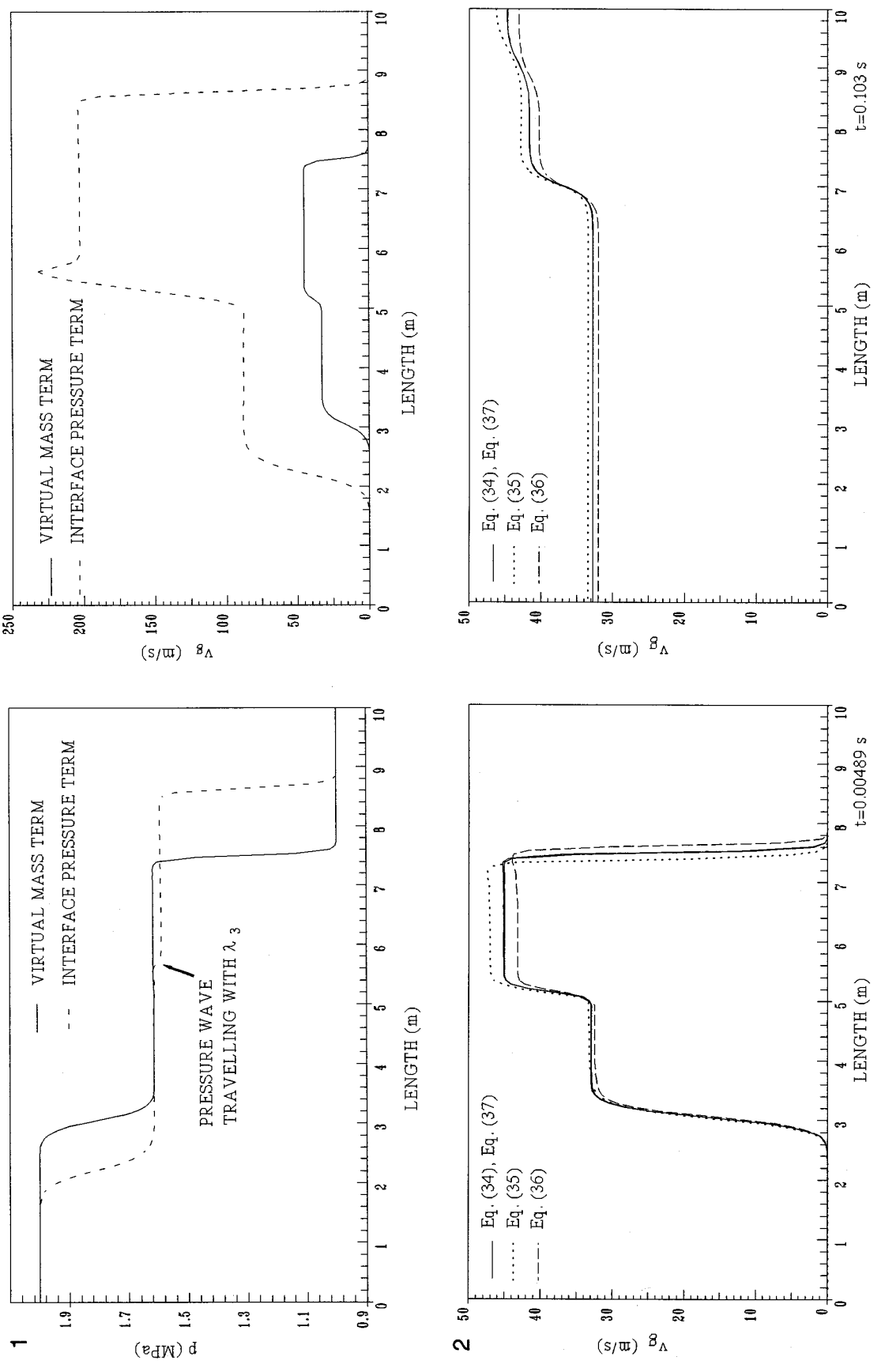

FIG. 1. Influence of the different additional differential terms on the pressure profile and vapour velocity ($t = 0.00489$ s).
FIG. 2. Influence of the averaging on the shock and rarefaction wave ($t = 0.00489$ s) and on the waves belonging to λ_3 to λ_6 ($t = 0.103$ s).

The structure of the third and fourth eigenvectors shows two interesting properties of the two-phase flow equations:

—The first is the degeneration of the third and fourth eigenvectors as relative velocity approaches zero: $v_r \to 0$. There are two possible solutions for this situation; the strict solution is to solve only five equations in the points where $v_r = 0$. In that case, a separate subroutine for the calculation of the eigenvalues and eigenvectors is needed. An additional complication in that case is the comparison of the characteristic variable gradients (Eq. (30)) between two points; one with a five-equation model and the other with a six-equation model. A much simpler solution is to maintain a small artificial relative velocity ($v_r = \max(v_r, 10^{-9})$ for positive v_r and $v_r = \min(v_r, -10^{-9})$ for negative v_r) for the calculation of the third and fourth eigenvalues and eigenvectors. Both methods were tested and practically the same results were obtained; i.e., the second simpler method with small artificial v_r can be used without loss of accuracy.

—The first component of the third and fourth eigenvectors is not equal to zero for nonzero relative velocity. This component corresponds to the propagation of the pressure disturbances (Eq. (22)) and that means that the pressure disturbance will not only propagate with the sonic characteristics λ_1 and λ_2 but also with the third and fourth characteristic velocities (Fig. 1). In realistic two-phase flows, in which relative velocities are not too high, pressure waves travelling with λ_3 and λ_4 are very weak and the main pressure disturbances propagate usually only with the sonic characteristics. Fifth and sixth eigenvectors are trivial and do not deserve special attention; it need only be mentioned that pressure, vapour volume fraction, and phasic velocity disturbances do not propagate with λ_5 and λ_6.

In the current version of our PDE2 code eigenvalues and eigenvectors are determined using a combination of the approximate analytical expressions (15), (16), where possible and CPU expensive numerical procedures in the area where error of the approximate eigenvalues is too large. If approximate expressions are used for $|v_f|, |v_g|, |v_r| < 0.05c$ and $|v_r| < 10\ m/s$ and numerical procedures are used otherwise, the maximal relative error of the approximate eigenvalues appears to be around 10^{-3}. In a realistic simulation, the conditions which allow for use of the approximate eigenvalues are fulfilled most of the time. Numerical calculation of the eigenvalues and eigenvectors was performed with the subroutines from the EISPACK library [26], which are capable of finding the eigenvalues and eigenvectors of an arbitrary matrix.

From the discussion above we can see that the behaviour of the two-fluid models strongly depends on the additional differential terms used. Each of the today's computer codes for the simulations of nuclear thermalhydraulics uses different additional differential terms. RELAP5 uses the virtual mass term and interface pressure term for stratified flows, CATHARE uses a different virtual mass term than RELAP5 and an interface pressure term in all flow regimes, TRAC code uses the third form of the virtual mass term. Figure 1 presents a comparison of the RELAP5 two-fluid model (1)–(6) with virtual mass term (10), (11), with Toumi's two-fluid model without virtual mass term and with interface pressure term (12) with $\delta_i = 1.01$. Pressure and vapour velocity profiles are shown for Toumi's shock tube [31]. Toumi's two-phase shock tube is a Riemann problem for two-fluid models. An infinite tube is filled with gas-liquid mixture with the left and right states defined as:

—left state: $\alpha = 0.25$, $p = 20$ MPa, $v_g = 0$ m/s, $v_f = 1$ m/s, $u_g = 2824$ kJ/kg, $u_f = 1311$ kJ/kg;

—right state: $\alpha = 0.1$, $p = 10$ MPa, $v_g = 0$ m/s, $v_f = 1$ m/s, $u_g = 2836$ kJ/kg, $u_f = 1330$ kJ/kg.

The membrane which separates left and right part of the tube at the position 5 m is removed at time zero. All nondifferential terms, i.e. sources, were neglected in both cases in order to get a better insight into the structure of the differential terms. Figure 1 thus **cannot** present a realistic physical situation. A significant difference can be seen between the speed of the waves for different additional differential terms. Relative velocities in the case with an interface pressure term are large (~200 m/s) and comparable with sonic velocities (~700 m/s), thus accuracy of the approximate expressions for the eigenvalues and eigenvectors is not sufficient, and numerical decomposition of the Jacobian matrix is used. The virtual mass term reduces sonic velocity and does not allow such large relative velocities as the interface pressure term.

Analysis of the eigenvalues and results in Fig. 1 shows the role of the additional differential terms in two-fluid models. Since different authors and codes use different additional differential terms it is clear that uncertainty of two-fluid models is significant. The uncertainty of the additional differential terms becomes less important in realistic two-phase flow models where source terms are included. Interphase exchange sources tend to establish mechanical and thermal equilibrium between both phases. These equilibrium states are equal, no matter which additional differential terms are used. As the interphase exchange source terms increase, the solutions of the two-fluid models with different additional differential terms become closer. Solutions of the two-fluid model with infinite interphase exchange sources would be equal to the solutions of the three-equation homogeneous-equilibrium model of two-phase flow [30]. While the importance of the uncertainty of the additional differential terms is decreased with the introduction of the source terms, inclusion of the sources introduces a new uncertainty which is even more important and is analyzed in Sections 9 and 10.

5. NUMERICAL METHOD

The PDE2 code used for solving the six-equation model of the two-phase flow with a second-order accurate scheme can be used for hyperbolic problems. The system of Eqs. (13) can be multiplied by $\mathbf{A}^{-1}$ from the left. If the sources, which are described in the next section, are omitted, we obtain

$$\frac{\partial \mathbf{\Psi}}{\partial t} + \mathbf{C}\frac{\partial \mathbf{\Psi}}{\partial x} = 0 \tag{19}$$

with $\mathbf{C} = \mathbf{A}^{-1}\mathbf{B}$ as Jacobian matrix. If the eigenvalues and eigenvectors of the matrix $\mathbf{C}$ are found by the methods described in Section 4, the Jacobian matrix can be written as

$$\mathbf{C} = \mathbf{L}\,\mathbf{\Lambda}\,\mathbf{L}^{-1}, \tag{20}$$

where $\mathbf{L}$ is a matrix of the eigenvectors and $\mathbf{\Lambda}$ the diagonal matrix of the eigenvalues. If expression (20) is taken into account in Eq. (19), and Eq. (19) multiplied by $\mathbf{L}^{-1}$ from the left, we obtain

$$\mathbf{L}^{-1}\frac{\partial \mathbf{\Psi}}{\partial t} + \mathbf{\Lambda}\mathbf{L}^{-1}\frac{\partial \mathbf{\Psi}}{\partial x} = 0. \tag{21}$$

The vector of the characteristic variables is introduced as

$$\delta\boldsymbol{\xi} = \mathbf{L}^{-1}\delta\mathbf{\Psi}, \tag{22}$$

where $\delta\boldsymbol{\xi}$ represents an arbitrary variation: $\partial\boldsymbol{\xi}/\partial t$ or $\partial\boldsymbol{\xi}/\partial x$. Equation (19) can be written in the characteristic form

$$\frac{\partial \boldsymbol{\xi}}{\partial t} + \mathbf{\Lambda}\frac{\partial \boldsymbol{\xi}}{\partial x} = 0. \tag{23}$$

An improved characteristic upwind discretization [11] of Eq. (23) with an explicit finite difference scheme is

$$\frac{\boldsymbol{\xi}_j^{n+1} - \boldsymbol{\xi}_j^n}{\Delta t} + (\mathbf{\Lambda}^+)_{j-1/2}^n \frac{\boldsymbol{\xi}_j^n - \boldsymbol{\xi}_{j-1}^n}{\Delta x} + (\mathbf{\Lambda}^-)_{j+1/2}^n \frac{\boldsymbol{\xi}_{j+1}^n - \boldsymbol{\xi}_j^n}{\Delta x} = 0 \tag{24}$$

and is first-order accurate in time and space. $\mathbf{\Lambda}^+$ is equal to the matrix $\mathbf{\Lambda}$ with negative eigenvalues set equal to zero, and $\mathbf{\Lambda}^-$ is equal to the matrix $\mathbf{\Lambda}$ with positive eigenvalues set equal to zero.

The Lax–Wendroff discretization [11] of Eq. (23) is second-order accurate in space and time:

$$\begin{aligned}\frac{\boldsymbol{\xi}_j^{n+1} - \boldsymbol{\xi}_j^n}{\Delta t} &+ \frac{1}{2}\left(\mathbf{\Lambda}_{j-1/2}^n + \left(\mathbf{\Lambda}_{j-1/2}^n\right)^2 \frac{\Delta t}{\Delta x}\right)\frac{\boldsymbol{\xi}_j^n - \boldsymbol{\xi}_{j-1}^n}{\Delta x} \\ &+ \frac{1}{2}\left(\mathbf{\Lambda}_{j+1/2}^n - \left(\mathbf{\Lambda}_{j+1/2}^n\right)^2 \frac{\Delta t}{\Delta x}\right)\frac{\boldsymbol{\xi}_{j+1}^n - \boldsymbol{\xi}_j^n}{\Delta x} = 0.\end{aligned} \tag{25}$$

A problem of the pure second-order accurate discretizations is presented by the oscillations which appear in the vicinity of the nonsmooth solutions. The problem is solved [23, 16] if the combination of the first- and second-order accurate discretizations is used. Part of the second-order discretization is determined by the so-called flux limiters [16] which ''measure'' the smoothness of the solutions. If the solutions are smooth, the larger part of the second-order discretization is used; otherwise the larger part of the first-order discretization is used.

The final discretization of Eq. (23) is

$$\frac{\boldsymbol{\xi}_j^{n+1} - \boldsymbol{\xi}_j^n}{\Delta t} + (\mathbf{\Lambda}^{++})_{j-1/2}^n \frac{\boldsymbol{\xi}_j^n - \boldsymbol{\xi}_{j-1}^n}{\Delta x} + (\mathbf{\Lambda}^{--})_{j+1/2}^n \frac{\boldsymbol{\xi}_{j+1}^n - \boldsymbol{\xi}_j^n}{\Delta x} = 0. \tag{26}$$

Elements of the diagonal matrices $\mathbf{\Lambda}^{++}$, $\mathbf{\Lambda}^{--}$ are calculated as

$$\lambda_k^{++} = \max(0, \lambda_k) + \frac{\phi_k \lambda_k}{2}\left(\lambda_k \frac{\Delta t}{\Delta x} - \frac{\lambda_k}{|\lambda_k|}\right), \quad k = 1, 6, \tag{27}$$

$$\lambda_k^{--} = \min(0, \lambda_k) - \frac{\phi_k \lambda_k}{2}\left(\lambda_k \frac{\Delta t}{\Delta x} - \frac{\lambda_k}{|\lambda_k|}\right), \quad k = 1, 6. \tag{28}$$

Different flux limiters ϕ_k are available in [16]. One of them is minmod limiter:

$$\phi_k = \max(0, \min(1, \theta_k)), \quad k = 1, 6, \tag{29}$$

where θ_k measures the ratio of the left and the right gradients in the grid point $j + 1/2$:

$$\theta_{k,j+1/2} = \frac{\xi_{k,j+1-m} - \xi_{k,j-m}}{\xi_{k,j+1} - \xi_{k,j}}, \quad m = \frac{\lambda_{k,j+1/2}}{|\lambda_{k,j+1/2}|}, \quad k = 1, 6,\ j = 1, N-1. \tag{30}$$

If Eq. (26) is transformed into basic variables we obtain a difference scheme that is used in PDE2 code,

$$\frac{\mathbf{\Psi}_j^{n+1} - \mathbf{\Psi}_j^n}{\Delta t} + \mathbf{C}_{j-1/2}^{++}\frac{\mathbf{\Psi}_j^n - \mathbf{\Psi}_{j-1}^n}{\Delta x} + \mathbf{C}_{j+1/2}^{--}\frac{\mathbf{\Psi}_{j+1}^n - \mathbf{\Psi}_j^n}{\Delta x} = 0, \tag{31}$$

with

$$\mathbf{C}_{j-1/2}^{++} = \mathbf{L}_{j-1/2}\mathbf{\Lambda}_{j-1/2}^{++}\mathbf{L}_{j-1/2}^{-1}, \quad \mathbf{C}_{j+1/2}^{--} = \mathbf{L}_{j+1/2}\mathbf{\Lambda}_{j+1/2}^{--}\mathbf{L}_{j+1/2}^{-1}. \tag{32}$$

Evaluation of the Jacobian matrix $\mathbf{C}_{j+1/2}$ from the values in the grid points j and $j+1$ is given in Section 8. A time step of the scheme is limited by the CFL (Courant–Friedrichs–Lewy) condition $\Delta t \leq \Delta x/\max(|\lambda_k|)$, $k = 1, 6$.

The described numerical scheme becomes a standard high-resolution shock-capturing method if:

—Eq. (19) can be written in conservative form,

—conservative variables are chosen as components of the vector $\mathbf{\Psi}$,

—the appropriate Riemann solver is applied for evaluation of the Jacobian matrix $\mathbf{C}$ in $j + 1/2$,

—an entropy fix is applied for genuinely nonlinear characteristic fields.

6. SOURCES

Integration of the sources in Eqs. (13) is performed in a separated step using Strang operator splitting [16] and the explicit second-order Euler method which allows variable time steps. Sources in the equations of the two-fluid model were divided into two groups in Section 2:

—Stiff source terms—terms describing interphase mass, momentum, and energy transfer which tend to establish mechanical ($v_r \to 0$) and thermal equilibrium ($T_f, T_g \to T_s$).

—Other terms which represent external forces (gravity, wall friction) and wall heat transfer.

LeVeque and Yee [18] have shown that stiff sources may affect the propagation of the discontinuities and produce spurious solutions. We have performed numerical tests which have shown that stiff sources describing interphase exchange in two-fluid models do not produce spurious solutions. The tests were performed with different source terms increasing their stiffness (increasing the heat transfer coefficients H_{if}, H_{ig} and interphase friction coefficient C_D by a few orders of magnitude). The results of the tests have shown that as the stiffness of the sources increases, the solutions of the two-fluid model tend toward the solution of the equilibrium equations. Equilibrium equations of the presented two-fluid model are three equations of the homogeneous equilibrium model of two-phase flow [30]. According to Pember's conjecture [20], this convergence is a sufficient condition which guarantees that the numerical method will not produce spurious solutions due to the stiff sources.

Stiff sources require integration with a time step, which can be much lower than the time step of the CFL condition. The time step for the integration of the sources is not constant and is controlled by the relative change of the basic variables. In one step of the integration, the maximal relative change of the basic variables allowed is 0.001. Additional criteria decrease the time step in order to prevent oscillations around the mechanical and thermal equilibrium state; i.e., the sign of the relative velocity must not change, and transition from subcooled to superheated, or the reverse, is not allowed due to the interphase exchange sources. The applied explicit integration may be very slow when the system is far from thermal or mechanical equilibrium and may require a few hundred time steps for one step of convection. However, as the system approaches equilibrium, the number of integration steps decreases rapidly, and for systems near equilibrium (at which most processes run) two to four steps are usually enough for the integration.

The effect of the sources from the second group is negligible in the calculations presented in this paper. However, stiffness of the neglected wall heat transfer sources cannot be excluded in advance in some extreme conditions in nuclear thermalhydraulics. Stiffness of the wall heat transfer sources would cause an additional problem for the numerical method and would require a careful treatment.

7. SINGLE TO TWO-PHASE FLOW TRANSITION

There are two types of single to two-phase flow transition, and they both require replacement of the three-equation model by a six-equation model:

(1) Convection of the two-phase flow into the single-phase region, which can occur in any type of two-phase flow is modelled by the first-order upwind scheme. Second-order corrections require comparison of the characteristic variables at neighbouring points. Three-equation model eigenvectors cannot be directly compared to six-equation model eigenvectors. An alternative approach, which improves the accuracy at such points, is treating of the single phase volumes as the two-phase volumes with a small artificial amount of the other phase (10^{-8}).

(2) The second type of single to two-phase flow transition is vaporization or condensation when saturation conditions are reached, which is present only for the flows in which phase changes are possible. Fast depressurization of the hot liquid is often met in transient analyses, while transients with rapid condensation of the gas phase—like condensation-induced water hammer—are not so often encountered, but are also important. The simplest model for such a transition (which is used in RELAP5 and in PDE2 code) is the introduction of a very small amount of the new phase when the saturation pressure is reached.

Equivalent problems that require comparable treatment appear during the two-phase to single-phase transition.

8. SIMULATIONS OF THE DISCONTINUOUS SOLUTIONS

Equations of the two-fluid model are derived from the instantaneous equations averaged over time and/or space.

They cannot be written in conservative form due to the pressure gradient terms multiplied by phasic volume fractions and the additional differential terms in the momentum equations. The question is, therefore, how to define the Rankine–Hugoniot conditions which provide necessary additional information at the points where solutions are discontinuous and how to define the entropy condition.

Part of the answer can be found in the work of Toumi [30–32]. In 1992 Toumi [30] presented a weak formulation of Roe's approximate Riemann solver [23] for conservation laws which cannot be written in the conservative form. He presented a technique for the construction of the Jacobian matrix for the equations written with the conservative variables between the points j and $j + 1$. Preliminary results for the six-equation model of two-phase flow with interface pressure term (12) were presented by Toumi in 1995 [31]. Toumi's technique becomes very complicated if the virtual mass term with temporal and spatial derivatives is used instead of the interface pressure term which contains spatial derivatives only. It turns out that for more complicated additional differential terms even evaluation of the Jacobian matrix for the conservative variables becomes a problem (see Section 8.1). Toumi concluded in 1996 [32] that "*the solution of Riemann problem is unknown for our nonconservative system*" and "*there is no theoretical background to ensure that computed shocks have always correct speeds.*"

In this paper we avoid the use of Toumi's approximate Riemann solver. We, rather, performed the calculations with different simple types of averaging between the neighbouring grid points and with different types of the basic variables. This section presents an estimate for the uncertainties due to the unknown Rankine–Hugoniot conditions and an inaccurate Riemann solver.

8.1. *Averaging*

According to Roe [23], the Jacobian matrix of Eq. (19) for the Riemann problem can be evaluated as an integral along the straight line linking states $\boldsymbol{\phi}_j$ and $\boldsymbol{\phi}_{j+1}$:

$$\mathbf{C}(\boldsymbol{\phi}_j, \boldsymbol{\phi}_{j+1}) = \int_0^1 \mathbf{C}(\boldsymbol{\phi}_j + s(\boldsymbol{\phi}_{j+1} - \boldsymbol{\phi}_j))\, ds. \tag{33}$$

Since the integrals (33) may not emerge in closed form, other techniques are usually used (Roe averaging [23], Toumi [30]), which ensure the correct speed of the discontinuities. The first method tested with the two-fluid model is a simple average for the evaluation of the state between the points j and $j + 1$. Arithmetic averaging used in the PDE2 code presents a simple approximation of Eq. (33):

$$\int_0^1 \mathbf{C}(\boldsymbol{\phi}_j + s(\boldsymbol{\phi}_{j+1} - \boldsymbol{\phi}_j))\, ds \approx \mathbf{C}((\boldsymbol{\phi}_j + \boldsymbol{\phi}_{j+1})/2). \tag{34}$$

The best results were obtained when $\boldsymbol{\phi}$ was a vector of nonconservative variables $\boldsymbol{\phi} = \boldsymbol{\Psi} = (p, \alpha, v_f, v_g, u_f, u_g)$. This type of averaging was recently tested by Gallouet [10] with Euler equations and standard Sod's shock tube problems. He presented an excellent agreement of the results calculated by the Roe approximate Riemann solver and with simple averaging (34) by averaging vector $\boldsymbol{\phi} = (p, v, \rho)$. He named this approach as a "rough Godunov method." He included the entropy fix, which is based on the entropy condition derived for a conservative system of equations. Gallouet did not offer any mathematical background for his method.

In addition to the arithmetic averaging (34), we applied LeVeque's scheme for a nonconservative systems of equations [17]. His method is equivalent to the evaluation of the matrix $\mathbf{C}$ eigenvalues in the grid points j and $j + 1$, and evaluation of the state in $j + \frac{1}{2}$ as a combination of the left and right eigenvalues and eigenvectors, depending on the eigenvalues sign:

$$\lambda_{k,j+1/2} = \begin{cases} \lambda_{k,j} & \lambda_{k,j} + \lambda_{k,j+1} < 0 \\ \lambda_{k,j+1} & \lambda_{k,j} + \lambda_{k,j+1} > 0, \end{cases}$$
$$\mathbf{l}_{k,j+1/2} = \begin{cases} \mathbf{l}_{k,j} & \lambda_{k,j} + \lambda_{k,j+1} < 0 \\ \mathbf{l}_{k,j+1} & \lambda_{k,j} + \lambda_{k,j+1} > 0. \end{cases} \tag{35}$$

The inverted LeVeque method was also tested,

$$\lambda_{k,j+1/2} = \begin{cases} \lambda_{k,j} & \lambda_{k,j} + \lambda_{k,j+1} > 0 \\ \lambda_{k,j+1} & \lambda_{k,j} + \lambda_{k,j+1} < 0, \end{cases}$$
$$\mathbf{l}_{k,j+1/2} = \begin{cases} \mathbf{l}_{k,j} & \lambda_{k,j} + \lambda_{k,j+1} > 0 \\ \mathbf{l}_{k,j+1} & \lambda_{k,j} + \lambda_{k,j+1} < 0, \end{cases} \tag{36}$$

as well as another type of arithmetic averaging,

$$\lambda_{k,j+1/2} = 0.5(\lambda_{k,j} + \lambda_{k,j+1}), \quad \mathbf{l}_{k,j+1/2} = 0.5(\mathbf{l}_{k,j} + \mathbf{l}_{k,j+1}). \tag{37}$$

Comparison of the results with the above four different types of averaging are shown in Fig. 2 for the equations with a virtual mass term and Toumi's shock tube from Section 4. Solutions calculated by both types of arithmetic averaging (34) and (37) are very similar and lie between the solutions with LeVeque's and inverted LeVeque's averaging, and so the results with averaging (35) and (36) can be treated as an estimate for the error made due to the inaccurate Riemann solver. This error is much lower than the uncertainty due to the additional differential terms (Fig. 1).

8.2. *Conservative and Nonconservative Variables*

Another test of the numerical method was made with the different vectors of the basic variables in Eq. (19). Equations of the two-fluid model written with conservative variables are still in nonconservative form. A conservative form does not exist for the momentum Eq. (3) and (4) due to the pressure gradient terms and additional differential terms. Total energy equations which are derived from the momentum equations (3), (4) and internal energy equations (5), (6) are also in nonconservative form. Only continuity equations (1), (2) can be written in the conservative form. A few test calculations have been thus performed with conservative variables in order to examine how the choice of the basic variables in the equations affects the solutions.

The Jacobian matrix of conservative variables contains very complicated expressions due to the additional differential terms and that makes the explicit expression for the Jacobian matrix for the conservative variables practically useless. Explicit evaluation of the Jacobian matrix has been avoided by the following procedure: the variation of the vector of the conservative variables,

$$\begin{aligned}\boldsymbol{\varphi} = [&(1-\alpha)\rho_f, \alpha\rho_g, (1-\alpha)\rho_f v_f, \alpha\rho_g v_g,\\ &(1-\alpha)\rho_f(u_f + v_f^2/2), \alpha\rho_g(u_g + v_g^2/2)],\end{aligned} \tag{38}$$

can be expressed with variation of the vector of the basic variables $\boldsymbol{\Psi} = (p, \alpha, v_f, v_g, u_f, u_g)$ as

$$\delta\boldsymbol{\varphi} = \mathbf{Q}\,\delta\boldsymbol{\Psi}, \tag{39}$$

with the transformation matrix

$$\mathbf{Q} = \begin{vmatrix} (1-\alpha)\dfrac{\partial\rho_f}{\partial p} & -\rho_f & 0 & 0 & (1-\alpha)\dfrac{\partial\rho_f}{\partial u_f} & 0\\ \alpha\dfrac{\partial\rho_g}{\partial p} & \rho_g & 0 & 0 & 0 & \alpha\dfrac{\partial\rho_g}{\partial u_g}\\ (1-\alpha)\dfrac{\partial\rho_f}{\partial p}v_f & -\rho_f v_f & (1-\alpha)\rho_f & 0 & (1-\alpha)\dfrac{\partial\rho_f}{\partial u_f}v_f & 0\\ \alpha\dfrac{\partial\rho_g}{\partial p}v_g & \rho_g v_g & 0 & \alpha\rho_g & 0 & \alpha\dfrac{\partial\rho_g}{\partial u_g}v_g\\ (1-\alpha)\dfrac{\partial\rho_f}{\partial p}\left(u_f+\dfrac{v_f^2}{2}\right) & -\rho_f\left(u_f+\dfrac{v_f^2}{2}\right) & (1-\alpha)\rho_f v_f & 0 & (1-\alpha)\left(\rho_f+\dfrac{\partial\rho_f}{\partial u_f}\left(u_f+\dfrac{v_f^2}{2}\right)\right) & 0\\ \alpha\dfrac{\partial\rho_g}{\partial p}\left(u_g+\dfrac{v_g^2}{2}\right) & \rho_g\left(u_g+\dfrac{v_g^2}{2}\right) & 0 & \alpha\rho_g v_g & 0 & \alpha\left(\rho_g+\dfrac{\partial\rho_g}{\partial u_g}\left(u_g+\dfrac{v_g^2}{2}\right)\right) \end{vmatrix} \tag{40}$$

With relation (39), Eq. (19) is transformed into

$$\frac{\partial\boldsymbol{\varphi}}{\partial t} + \mathbf{QCQ}^{-1}\frac{\partial\boldsymbol{\varphi}}{\partial x} = 0. \tag{41}$$

The eigenvector and inverse eigenvector matrices are then transformed:

$$\mathbf{L} \to \mathbf{QL}, \quad \mathbf{L}^{-1} \to \mathbf{L}^{-1}\mathbf{Q}^{-1}. \tag{42}$$

With such an approach the same numerical method described in Section 5 can be used for equations written with conservative and nonconservative variables. Additional tasks, in comparison to the nonconservative variables case, are evaluations of the matrices $\mathbf{Q}$ and $\mathbf{Q}^{-1}$ and transformations (42). CPU time consumption is only slightly increased, but the advantage of this approach is that the same eigenvalue and eigenvector subroutines can be used as in the nonconservative case.

The most important additional task, which is very demanding from the standpoint of the CPU time consumption, is evaluation of the equations of state: the pressure and vapour volume fraction have to be determined from the conserved quantities:

$$\begin{aligned} p &= p((1-\alpha)\rho_f, \alpha\rho_g, (1-\alpha)\rho_f(u_f + v_f^2/2), \alpha\rho_g(u_g + v_g^2/2)),\\ \alpha &= \alpha((1-\alpha)\rho_f, \alpha\rho_g, (1-\alpha)\rho_f(u_f + v_f^2/2), \alpha\rho_g(u_g + v_g^2/2)). \end{aligned} \tag{43}$$

A very expensive iterative procedure is used in the conservative variables code since pressure and specific internal energy are required as input parameters for the RELAP5 water property subroutines. Efficient use of the presented schemes with the conservative variables would require new water property subroutines with conservative variables as input and p, α as output parameters.

Figure 3 presents a comparison of the vapour velocities calculated with conservative variables (38), nonconservative variables, and with the third set of the so-called mixed variables:

$$\boldsymbol{\vartheta} = ((1-\alpha)\rho_f, \alpha\rho_g, v_f, v_g, (1-\alpha)\rho_f(u_f + v_f^2/2), \alpha\rho_g(u_g + v_g^2/2)), \tag{44}$$

where the continuity and energy equations are written with conservative variables and the momentum equations with nonconservative variables. Only the vapour velocity is presented in Fig. 3, while the other variables show a similar behaviour. Toumi's shock tube case and two-fluid model with a virtual mass term and without sources has been used on a grid of 150 cells and $\Delta t = 9.5 \times 10^{-5}$ s. Arithmetic averaging (34) was used in all cases.

Similar rarefraction and shock waves are predicted in all three cases in Fig. 3, while nonphysical oscillation in the "conservative variables" solution can be observed for other waves. Such oscillations are not the common oscillations associated with high order numerical schemes and were first observed in the modelling of multicomponent flows. Karni, 1994 [14] and Abgrall, 1996 [1] analyzed the dynamics of an inviscid two-component mixture of ideal gases described by three Euler equations and an additional equation for the concentration of one component. Oscillations near the contact discontinuity occur in the solutions of the two-component model when the material properties are different on each side of the discontinuity and standard Roe-type numerical schemes are applied. Karni [14] has shown that these oscillations are avoided if the three Euler equations are written with nonconservative variables (p, v, ρ). He presented a numerical scheme with nonconservative variables and with correction which reduces the nonconservation error near the discontinous solutions.

The behaviour of the six-equation two-fluid model is more complex than that of the four-equation two-component model. This is shown in Fig. 4, where the vapour velocity profile was calculated with Toumi's shock tube initial conditions, but with a higher vapour volume fraction in the left side of the tube $\alpha_L = 0.9$ (instead of 0.25 as in Figs. 1–3). Figure 4 shows that solving the equations with nonconservative variables also produces a nonphysical oscillation; not in the contact discontinuity but in the shock and rarefaction wave. The oscillations in Figs. 3 and 4 have a similar source. Figure 4 shows the advantage of the equations written with mixed variables (44)—oscillations are avoided if conservative variables are used for the mass and energy equations and nonconservative variables are used for the momentum equations. The results of the conservative variables are not shown in Fig. 4; simulation was not possible due to the very strong oscillations near the contact discontinuities.

We may conclude that the choice of the different basic

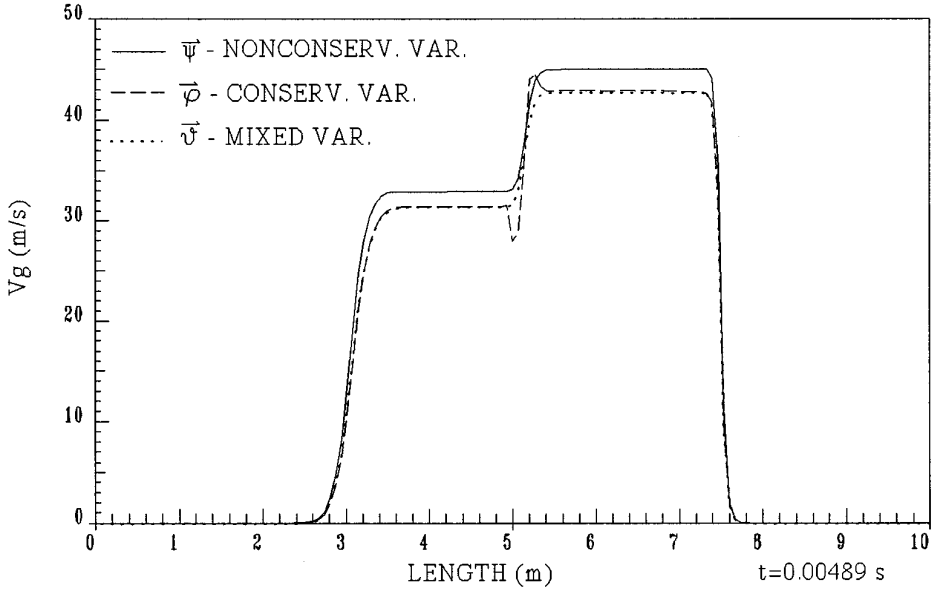

FIG. 3. Influence of the different basic variables on the Toumi's shock-tube problem solution at time $t = 0.00489$ s ($\alpha_L = 0.25$, $\alpha_R = 0.1$).

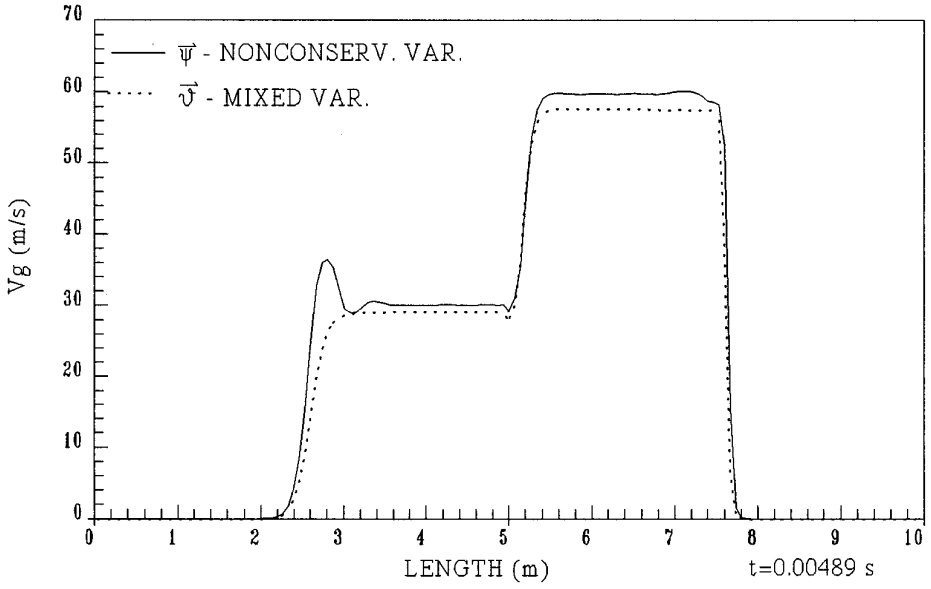

FIG. 4. Influence of the different basic variables on the shock-tube problem solution at $t = 0.00489$s. Large initial vapour void fraction jump: $\alpha_L = 0.9$, $\alpha_R = 0.1$.

variables does not have a significant impact on the continuous solutions of the equations. However, differences can appear around the strong discontinuities. Two types of errors can occur in such points:

—*Oscillations at the material interfaces.* These can cause significant problems when the equations are solved with conservative variables. The equations solved with nonconservative variables can also produce some weaker oscillations near the shock and rarefaction waves, while the oscillation-free results were obtained with mixed variables (44).

—A second type of error near the discontinuities is a *nonconservation error*. This error requires careful control of the overall mass and energy when the transients are simulated with nonconservative variables. The entropy fix has to be applied for the elimination of the discontinuities that violate the entropy conditions.

Uncertainty due to the inaccurate Riemann solver is not negligible. However, comparison of Figs. 2–4 and Fig. 1 shows that the Riemann solver uncertainty is small, compared to the uncertainties in the additional differential terms. As will be shown in the following sections, the Riemann solver uncertainty is also small compared to the uncertainties in the source terms. From that point of view, arithmetic averaging (34) seems to be an acceptable approximation for the evaluation of the Jacobian matrix.

9. SHOCK-TUBE RESULTS

Toumi's two-phase shock tube problem [31]—the Riemann problem for the two-fluid model—has been defined in Section 4. Figures 1–4 in the previous sections present the results for unrealistic two-phase flow without source terms in the equations. The grid in Figs. 1–4 has 150 volumes and $\Delta t = 9.5 \times 10^{-5}$ s. The results shown in Fig. 5 are obtained by a two-fluid model with a virtual mass term, nonconservative variables, and the omitted source terms. The figure presents the total energy profiles for Toumi's shock tube with a membrane at 2.5 m, $\Delta t = 5.6 \cdot 10^{-5}$ s $= 0.96\Delta t_{CFL}$, grid 300 volumes, and a highly compressive superbee flux limiter [16]. A first-order accurate solution (limiters in Eq. (29) are set equal to zero) is added in Fig. 5 in order to check the advantage of the second-order accurate schemes. The solution at time 0.00417 s in Fig. 5 contains a shock wave, a rarefaction wave, and a wave which contains four waves belonging to λ_3 to λ_6. The total energy profile in Fig. 5 at time 0.1625 s contains the other four waves, while the shock wave and the rarefaction wave at that time travel beyond the observed pipe length. As expected, the solution of the Riemann problem for six equations consists of seven constant states separated by six waves.

Figures 6 and 7 present the importance of the source terms in the two-fluid models. The PDE2 pressure and vapour volume fraction on Figs. 6 and 7 were calculated for Toumi's shock tube, with and without source terms. The pressure profile at time 0.00489 s shows the lower shock and rarefaction wave speeds when the sources are included. The pressure calculated with the sources at time 0.1027 s in Fig. 7 is lower than the "no sources" pressure at that time due to the initial thermal nonequilibrium between both phases, which gradually vanishes. Due to the

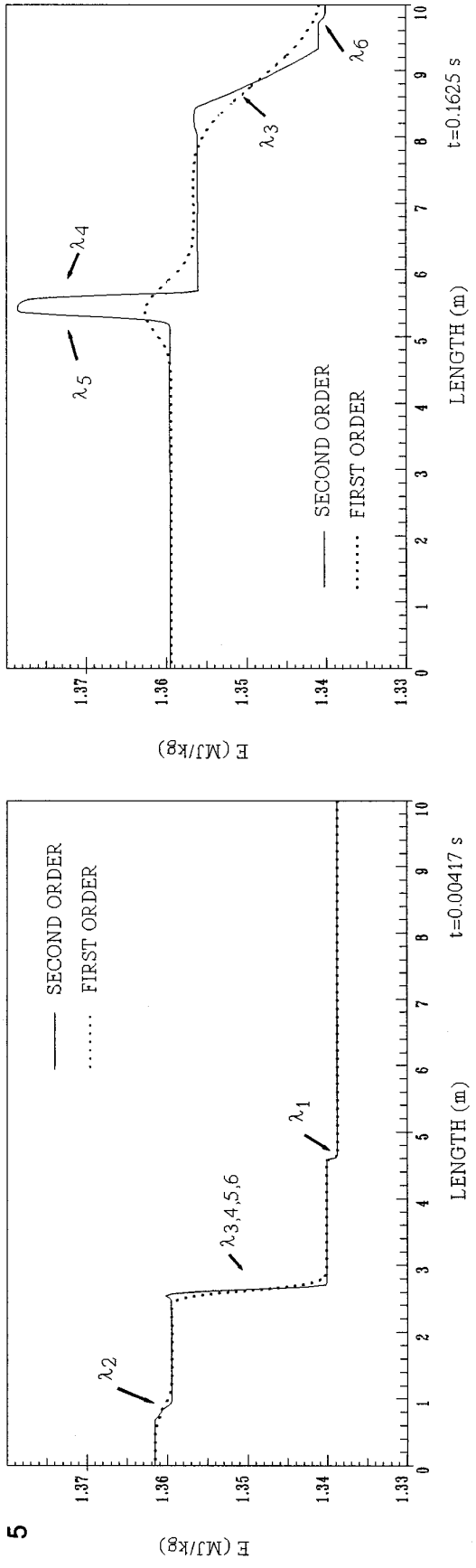

FIG. 5. Total energy profiles at $t = 0.00417$ s and $t = 0.1625$ s.

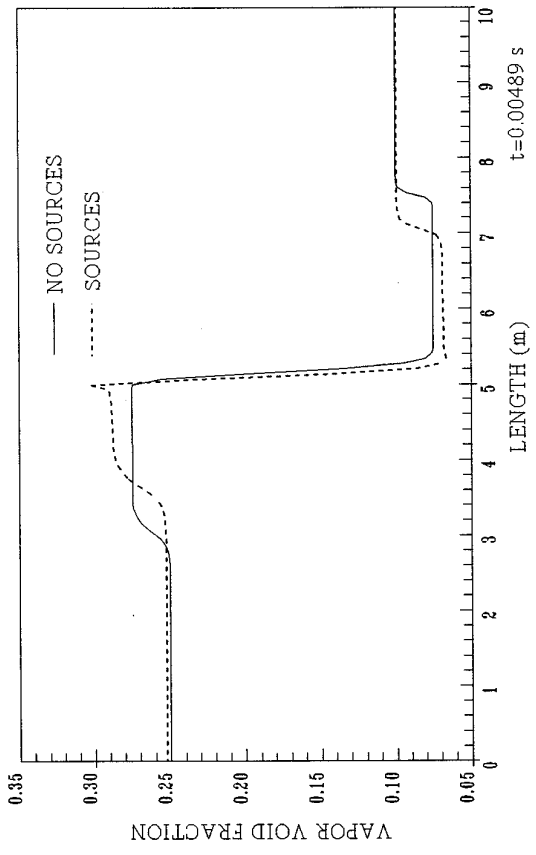

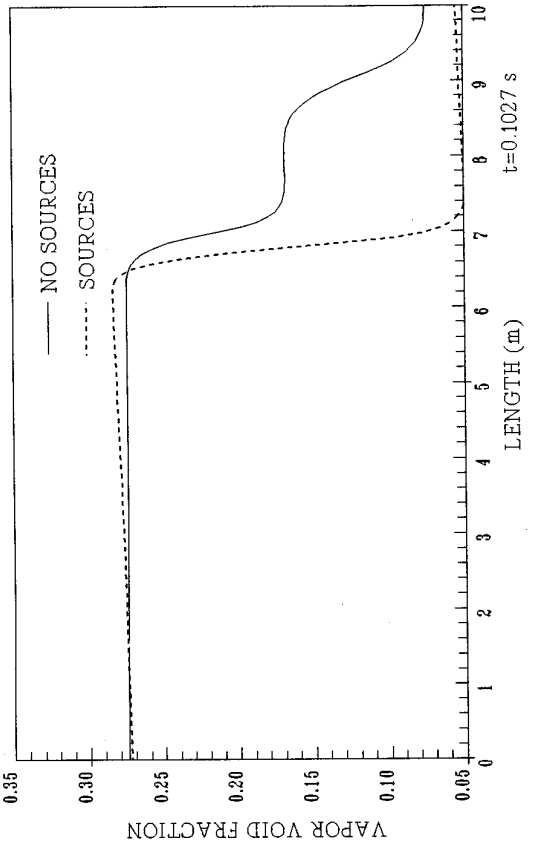

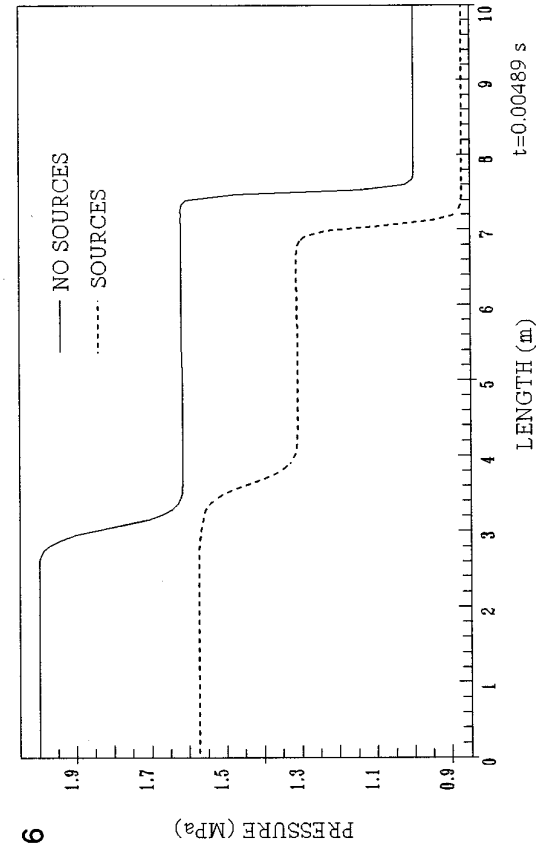

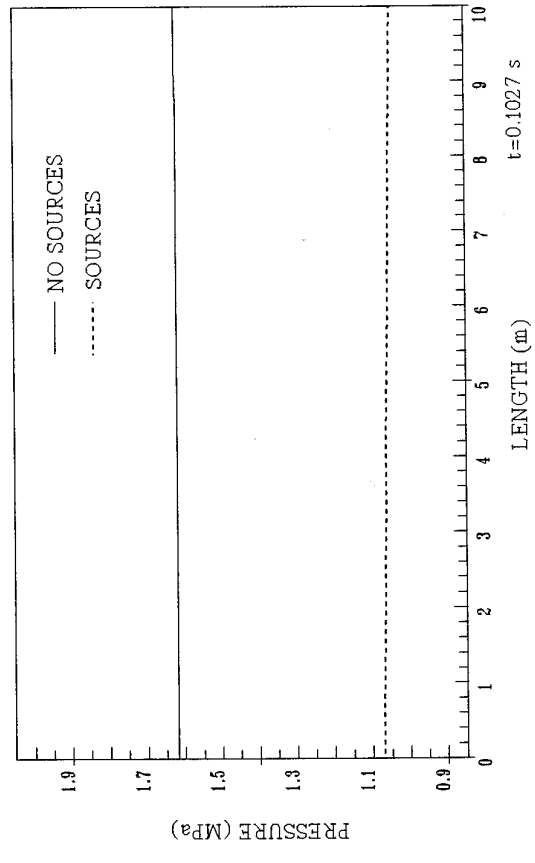

FIG. 6. Pressure and vapour volume fraction at $t = 0.00489$ s. Comparison of Toumi's shock tube with and without sources.
FIG. 7. Pressure and vapour volume fraction at $t = 0.1027$ s. Comparison of Toumi's shock tube with and without sources.

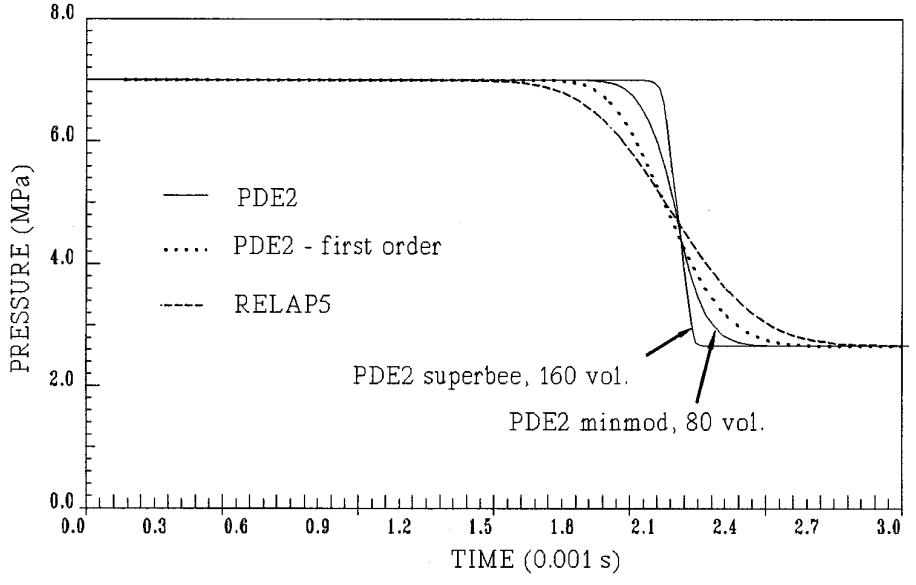

FIG. 8. Calculated pressure history 1.5 m from the closed end of the pipe in the first 0.003 s.

momentum interphase transfer, relative interphase velocity is much lower than in the case without sources. That means that four very similar eignevalues exist, and splitting of the vapour volume fraction "contact discontinuity" into two waves is very weak compared to the "no source" case. A single wave visible at time 0.1027 s, in fact, contains two waves which are not well separated.

10. EDWARDS PIPE RESULTS

The Edwards pipe experiment [9] is used as one of the basic benchmarks for the two-phase flow codes due to its simple geometry and the wide range of phenomena that it covers. Edwards and O'Brien filled a 4-m long pipe, cross section 0.00456 m^2, with liquid water at 7 MPa and 502 K and suddenly ruptured one end of the tube (break cross section 0.00397 m^2). They measured pressures and vapour volume fractions during the blowdown at a few points along the pipe axis. Important phenomena observed were: pressure rarefaction wave, flashing onset, critical two-phase flow, and vapour volume fraction wave.

The results in Figs. 8–11 were predicted by RELAP5, second-order PDE2 code with minmod limiter, and first-order PDE2 code. Nonconservative variables have been

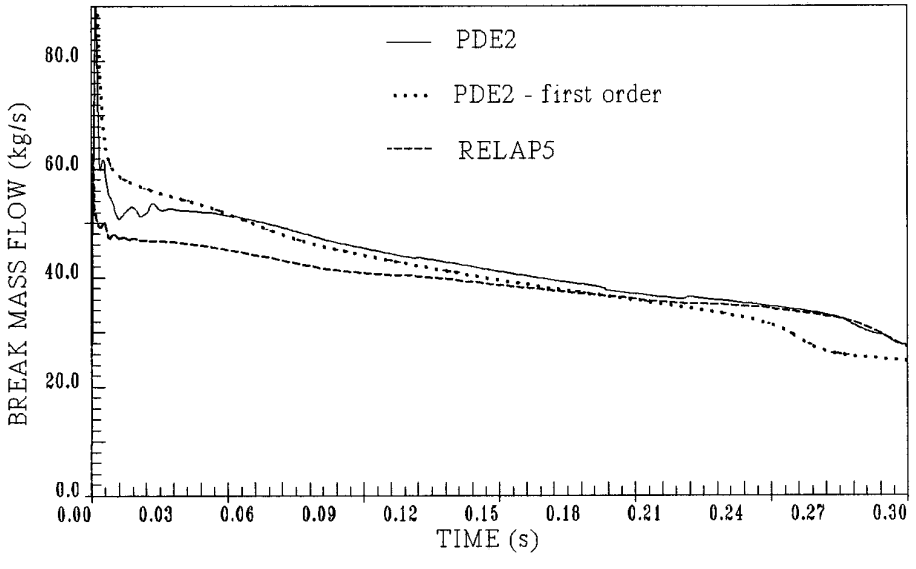

FIG. 9. Break flow predicted by PDE2 codes and RELAP5.

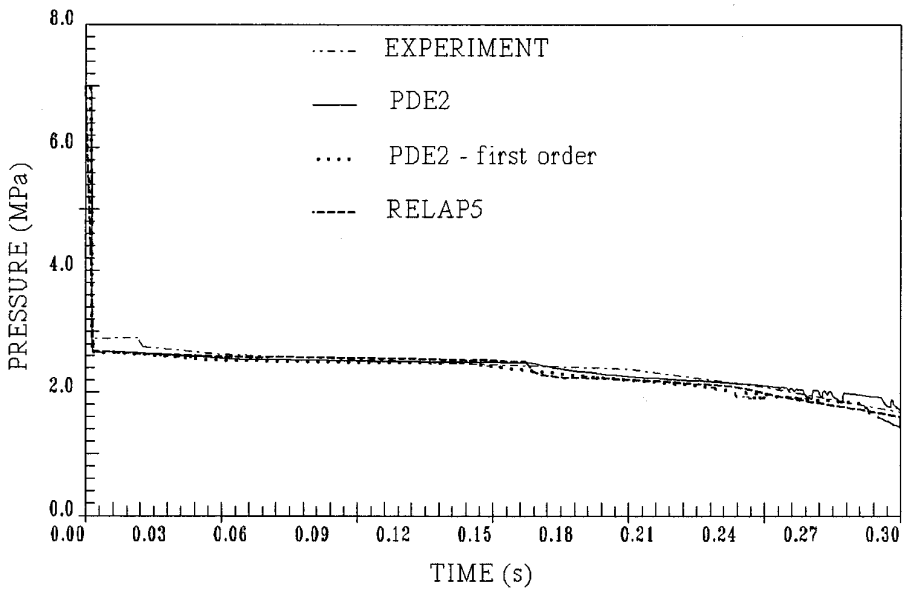

FIG. 10. Measured and calculated pressure history 1.5 m from the closed end of the pipe.

used in the PDE2 calculations. Grid-independent results were obtained with the discretization of the pipe into 80 volumes ($\Delta x = 5cm$), except for the pressure rarefaction wave on Fig. 8. The width of the rarefaction wave is very low, since the wave travels through the single phase liquid. An accurate description would require a grid with $\Delta x \approx$ 1 mm (the estimate is based on the analytical solution of the single-phase Riemann problem [11]). The steepest rarefaction wave on Fig. 8, calculated with second-order PDE2 code with the superbee limiter and the grid of 160 volumes, is thus still too wide.

There are two main differences in the mathematical models of PDE2 and RELAP5 codes which are responsible for differences between RELAP5 and first-order PDE2 results (codes with different numerical schemes of the same accuracy):

(1) *Flow through the break.* PDE2 code predicts the critical flow through the break from the basic equations. An artificial rapidly diverging nozzle has been added behind the break in PDE2 simulations which enables critical flow calculations to be made. The nozzle was large enough

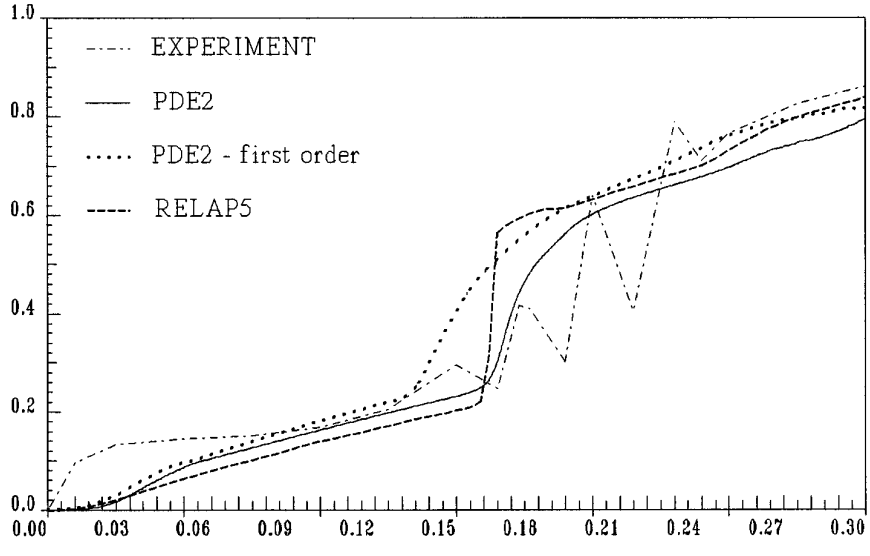

FIG. 11. Measured and calculated vapour void fraction 1.5 m from the closed end of the pipe.

and, thus, it did not affect the behaviour inside the pipe due to the flow choking at the break point. RELAP5 cannot predict the critical flow from the basic equations of the two-fluid model because its numerical scheme is not suitable for that purpose [29]. A simplified model is used instead, which is derived from simplified mathematical models and empirical correlations [34]. Figure 9 shows the RELAP5 and PDE2 break flows.

(2) Correlations for slug and annular flow regimes were neglected in the PDE2 simulations, and less accurate interpolation between the bubbly and droplet regimes has been used.

The expected differences between the first- and second-order PDE2 results are seen in Figs. 8–11—the waves predicted by the second-order scheme are steeper. The agreement between measured and calculated pressure histories at the point 1.5 m from the closed end of the pipe (Fig. 10) is very good; however, this is an expected result since the pressure is always about the saturation values in dispersed flows due to the rapid interphase mass and heat transfer. Significant differences, which stem from the nonaccurate closure laws, can be seen in the vapour volume fraction at the same point (Fig. 11). The first discrepancy is encountered at the beginning of the transient (0–0.03 s), where rapid measured increase of the vapour volume fraction was not predicted by RELAP5 or PDE2 codes. An additional discrepancy occurs at times 0.16 s–0.25 s, where measured vapour volume fraction wave contains a few oscillations which cannot be seen in any of the models. Except for the rarefaction wave predicted on Fig. 8, Figs 9–11 show that the uncertainties of the mathematical model are larger than the accuracy improvement due to the second-order accurate scheme in Edwards pipe modelling.

11. CONCLUSIONS

A second-order accurate scheme based on high-resolution shock-capturing methods was used for the simulation of the 1D two-fluid model of vapour–liquid flow. The hyperbolicity of the two-fluid model required by the presented numerical scheme was achieved with an appropriate form of the additional differential terms in the momentum equations. The eigenvalues and eigenvectors of the two-fluid model were calculated using a combination of the approximate expressions for low and moderate relative velocities and numerical procedures for high relative velocities. Special treatment was used for the zero relative velocities, where two of the eigenvectors degenerated into a single one. The sources were treated by Strang operator splitting. Integration of the stiff interphase exchange source terms required time steps shorter than the convection time step. Stiff interphase exchange sources did not produce spurious solutions.

It was shown that additional differential terms have a strong impact on the behaviour of the equations and on their solutions in the area of fast transients. Additional differential terms are less important in the area of slow (nonacoustic) transients, where the source terms play a major role and thermal and mechanical nonequilibrium between phases is small.

The nonconservative form of the equations and the absence of the Rankine–Hugoniot conditions for the two-fluid models may be a problem when discontinuous solutions are present. It was shown that the error introduced by the numerical scheme due to inaccurate treatment of the discontinuities is relatively small, compared to the uncertainty of the equations, and that simple averaging may be sufficient for the evaluation of the two-fluid model Jacobian matrix.

The results of the two-phase shock-tube problem and the Edwards pipe problem show significant uncertainties in the mathematical models of the general two-phase flow which are usually larger than the uncertainties of the applied numerical schemes. The results show important advantages of the second-order schemes in the area of fast transients with acoustic waves. For long lasting transients, where source terms play a major role, the advantages of the second-order schemes are of minor importance. In that case, the uncertainties of the closure laws in the source terms become much larger than the numerical diffusion errors of the first-order schemes. Second-order accurate schemes have prospects in the area of transients, where waves have to be traced and numerical diffusion has to be reduced. Second-order schemes will also be useful for developing new mathematical models and closure laws in two-phase flows, where numerical errors will have to be reduced as much as possible.

REFERENCES

1. R. Abgrall, How to prevent pressure oscillations in multicomponent flow calculations: A quasi conservative approach, *J. Comput. Phys.* **125,** 150 (1996).
2. G. S. Arnold, D. A. Drew, R. T. Lahey Jr., An assessment of multiphase flow models using the second law of thermodynamics, *Int. J. Multiphase Flow* **16,** 481 (1990).
3. D. Bestion, The physical closure laws in the CATHARE code, *Nucl. Eng. and Des.* **124,** 229 (1990).
4. M. Bottoni and W. Sengpiel, *Review of Mathematical and Physical Basis of Two-Phase Flow Modelling,* KfK report 4759, Karlsruhe, 1992.
5. G. G. Brucker and E. M. Sparrow, Direct contact condensation of steam bubbles in water at high pressure, *Int. J. Heat Mass Transfer* **20,** 371 (1977).
6. K. E. Carlson, R. A. Riemke, S. Z. Rouhani, R. W. Shumway, and W. L. Weaver, *RELAP5/MOD3 Code Manual*, Vols. 1–7, NUREG/CR-5535, EG&G Idaho, Idaho Falls, 1990.
7. C. F. Colebrook, Turbulent flow in pipes with particular reference

to the transition region between smooth and rough pipe laws, *Journal of Institute of Civil Engineers* **11,** 133, 1939.

8. D. Drew, L. Cheng, and R. T. Lahey Jr., The analysis of virtual mass effects in two-phase flow, *Int. J. Multiphase Flow* **5,** 233 (1979).
9. A. R. Edwards, F. P. O'Brien, Studies of phenomena connected with the depressurization of water reactors, *J. of the Br. Nucl. Soc.* **9,** 125 (1970).
10. T. Gallouet and J. M. Masella, A rough Godunov scheme, *C.R.A.S Paris* **323,** 77 (1996).
11. C. Hirsch, *Numerical Computation of Internal and External Flows,* Vols. 1, 2 (Wiley, New York, 1988).
12. M. Ishii, *Thermo-fluid Dynamic Theory of Two-Phase Flow* (Eyrolles, Paris, 1975).
13. M. Ishii and T. C. Chawla, Local Drag Laws in Dispersed Two-Phase Flow, *NUREG/CR-1230,* **ANL-79-105,** 1979.
14. S. Karni, Multicomponent flow calculations by a consistent primitive algorithm, *J. Comput. Phys.* **112,** 31 (1994).
15. L. Lee, D. J. Ryley, The evaporation of water droplets in superheated steam, *Journal of Heat Transfer, ASME* **445,** 1968.
16. R. J. LeVeque, *Numerical Methods for Conservation Laws* (Birkhauser, Basel, 1992). [Lectures in Mathematics, ETH, Zurich]
17. R. J. LeVeque, *CLAWPACK User Notes* (University of Washington, Seattle, 1995).
18. R. J. LeVeque and H. C. Yee, A study of numerical methods for hyperbolic conservation laws with stiff source terms, *J. Comput. Phys.* **86,** 187 (1990).
19. K. W. McQuillan and P. D. Whalley, Flow patterns in vertical two-phase flow, *Int. J. Multiphase Flow* **11,** 161 (1985).
20. R. B. Pember, Numerical methods for hyperbolic conservation laws with stiff relaxation I. spurious solutions, *SIAM J. Appl. Math.* **53,** No. 5, 1293 (1993).
21. S. Petelin, I. Tiselj, Simulation of the decompression wave with RELAP5 program, in *ASME Winter Annual Meeting, New Orleans, 1993.* [*Unsteady Flows* **29** (1993)]
22. M. S. Plesset and S. A. Zwick, The growth of vapor bubbles in superheated liquids, *J. Appl. Phys.* **25**(4), 493 (1954).
23. P. L. Roe, Approximate Riemann solvers, parameter vectors, and difference schemes, *J. Comput. Phys.* **43,** 357 (1981).
24. W. T. Sha, S. L. Soo, On the Effect of $P\nabla\alpha$ Term in Multiphase Mechanics, *Int. J. Multiphase Flow* **5,** 153 (1979).
25. L.A.S. Shieh, R. Krishnamurty, and V. H. Ransom, Stability, accuracy, and convergence of the numerical methods in RELAP5/MOD3, *Nucl. Sci. Eng.* **116,** 227 (1994).
26. B. T. Smith et al., *Matrix Eigensystem Routines—EISPACK Guide,* 2nd ed., vol. 6 of Lecture Notes in Computer Science, (New York, Springer-Verlag, 1976).
27. A. Stritar, B. Mavko, A. Prošek, The best estimate analysis of large loss of coolant accident with uncertainty evaluation, *Trans. ANS* **66,** 584 (1992).
28. I. Tiselj, S. Petelin, Second order numerical method for two-fluid model of air-water flow, *Proceedings of the Nuclear Society of Slovenia Annual Meeting, Portorož* (1995).
29. I. Tiselj, S. Petelin, Verification of the RELAP5 equations with the flashing flow in the nozzle, *Validation of System Transient Analysis Codes, ASME 1995 Hilton Head Island, FED-Vol. 223,* 1995.
30. I. Toumi, A weak formulation of Roe's approximate Riemann solver, *J. Comput. Phys.* **102,** 360 (1992).
31. I. Toumi, An implicit second order numerical method for two-fluid models, *ICONE 3 Proceedings, Kyoto,* 1995.
32. I. Toumi, A. Kumbaro, An approximate linearized Riemann solver for a two-fluid model, *J. Comput. Phys.* **124,** 286 (1996).
33. *TRAC-PF1/MOD1: An Advanced Best-Estimate Computer Program for Pressurized Water Reactor Thermal-Hydraulic Analysis,* NUREG/CR-3858, L.A-10157-MS, 1986.
34. J. A. Trapp, V. H. Ransom, A choked-flow calculation criterion for nonhomogeneous, nonequilibrium, two-phase flow, *Int. J. Multiphase Flow* **8,** 669 (1982).
35. J. A. Trapp, R. A. Riemke, A nearly-implicit hydrodynamic numerical scheme for two-phase flows, *J. Comput. Phys.* **66,** 62 (1986).
36. H. C. Unal, Maximum bubble diameter, maximum bubble-growth time and bubble growth rate during the subcooled nucleate flow boiling of water up to 17 MN/m^2, *Int. J. Heat Mass Transfer* **19,** 643 (1976).
37. G. B. Wallis, *One-Dimensional Two-Phase Flow,* (McGraw-Hill Book Company, 1969).
38. N. Zuber, On the dispersed two-phase flow in the laminar flow regime, *Chem. Eng. Sci.* **19,** 897 (1964).